β-FeOOH nanorod as a highly active and durable self-repairing anode catalyst for alkaline water electrolysis powered by renewable energy

Yoshiyuki Kuroda,[1,2*] Shohei Takatsu,[1] Tatsuya Taniguchi,[3] Yuta Sasaki,[3] Ikuo Nagashima,[3] Akihiko Inomata,[3] Yoshinori Nishiki,[4] Awaludin Zaenal,[4] Takaaki Nakai,[4] Akihiro Kato,[4] Shigenori Mitsushima[1,2]

[1]Department of Chemistry Applications and Life Science, Graduate School of Engineering Science, Yokohama National University, 79-5 Tokiwadai, Hodogaya-ku, Yokohama, Kanagawa 240-8501, Japan.
[2]Advanced Chemical Energy Research Center, Institute of Advanced Sciences, Yokohama National University, 79-5 Tokiwadai, Hodogaya-ku, Yokohama, Kanagawa 240-8501, Japan.
[3]Kawasaki Heavy Industries Ltd., 1-1 Kawasaki-cho, Akashi, Hyogo 673-8666, Japan.
[4]De Nora Permelec Ltd., 2023-15 Endo, Fujisawa, Kanagawa 252-0816, Japan.

*Corresponding author: E-mail: kuroda-yoshiyuki-ph@ynu.ac.jp

ORCID ID
Yoshiyuki Kuroda: orcid.org/0000-0001-6095-0313
Shigenori Mitsushim: orcid.org/0000-0001-9955-2507

Abstract

A β-FeOOH nanorod was investigated as a highly active and durable self-repairing anode catalyst for alkaline water electrolysis with repeated potential change, simulating power from renewable energy. The β-FeOOH nanorod was synthesized by coprecipitation, using an organic buffer of tris(hydroxymethyl)aminomethane. The β-FeOOH nanorods dispersed in 1 M KOH aq. as an alkaline electrolyte were electrochemically deposited on a nickel electrode by a constant current electrolysis. The deposited β-FeOOH nanorods formed bundled network on the surface of the electrode and exhibited high oxygen evolution reaction (OER) activity, where the minimum OER overpotential was 285 mV at 100 mA cm^{-2}. The durability of the nickel electrode coated with β-FeOOH nanorods were tested via shutdown-based accelerated durability test, where electrolysis at 600 mA cm^{-2} for 1 min and the potential control at 0.5 V vs. reversible hydrogen electrode (RHE) for 1 min are repeated in the presence of β-FeOOH nanorod in the electrolyte. The catalyst coated electrode showed the low OER overpotential for 4000 cycles, whereas the OER overpotential of a bare nickel electrode increased within only 200 cycles. The β-FeOOH nanorod efficiently suppressed the corrosion of the nickel substrate and the layer of β-FeOOH nanorod was continuously repaired by accumulating the β-FeOOH nanorod from the electrolyte. Therefore, the β-FeOOH nanorod is useful as a self-repairing anode catalyst with high OER activity and durability.

Keywords

Iron oxyhydroxide, colloidal dispersion, alkaline water electrolysis, renewable energy, self-repair, durability test

Highlights

- β-FeOOH nanorod is synthesized via coprecipitation in the presence of organic buffer.
- Quite low overpotential for oxygen evolution reaction (285 mV at 100 mA cm^{-2}) was achieved.
- The catalyst layer was self-repaired to show high durability under accelerated durability test.

Graphical abstract

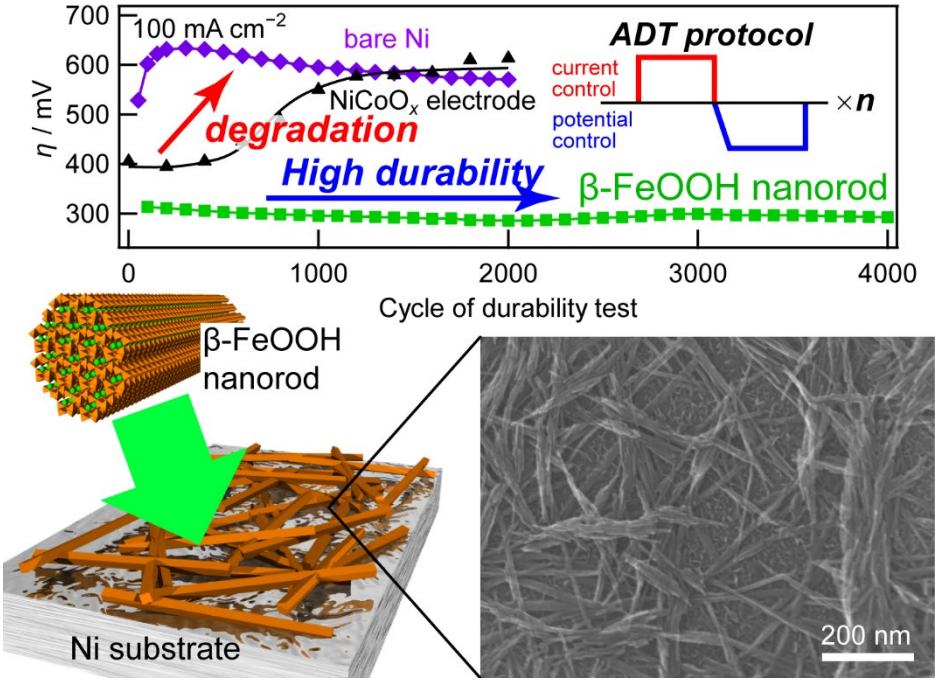

1 Introduction

To change our energy source from fossil fuels to renewable energy, the production of H_2 as an energy carrier by water electrolysis powered by renewable energy is highly demanded [1]. Alkaline water electrolysis (AWE) [2] and proton exchange membrane water electrolysis (PEMWE) [3] are currently major types of water electrolysis technologies. Although the efficiency of PEMWE is much higher than that of AWE, PEMWE requires a large amount of noble metals, such as Pt for cathode and Ir for anode because of the corrosion of base metals under acidic conditions. The use of noble metals must be reduced because of both high cost and scarcity. AWE is useful for this purpose because various base metals, such as Ni, Co, and Fe, can be used as electrode materials [4]. Furthermore, anion exchange membrane water electrolysis (AEMWE) is a promising as a possible solution to achieve both high efficiency and reduced usage of noble metals. Therefore, AWE is important to promote large scale hydrogen production from renewable energy.

Although AWE is quite stable under a constant power, degradation of electrodes is induced under frequent start and stop due to renewable energy. For example, when a bipolar alkaline water electrolyzer is operated, oxidation and reduction of anode and cathode, respectively, occur together with oxygen and hydrogen evolution reactions. On the suspension of the electrolyzer, the anode and cathode on the neighboring cells are short-circuited through a bipolar plate and electrolyte in the manifold. Thus, reverse current flows due to the discharge of the electrodes. The reverse current causes significant change in the electrode potentials, which promotes degradation of an electrode, such as corrosion of a substrate, detachment of electrocatalysts, and dissolution of electrocatalysts [5-7]. The start/stop operation and gas crossover of AEMWE may also cause degradation of electrode materials [8].

Because the oxygen evolution reaction (OER) has sluggish kinetics, the development of highly active and durable anode is one of the most important issues in the field of AWE [9]. To achieve highly durable anode under frequent potential change, the coating of a nickel electrode with a conductive metal oxides, such as Li-doped NiO is useful to protect the metal substrate from corrosion, though the OER activity of the coating was somewhat lower than an activated nickel electrode [10, 11]. It has been reported that stainless-steel is an active electrode durable under frequent potential change [12-14]. Recently, Ventosa et al. [15] and we [16] have reported a concept of self-repairing catalysts, where a catalyst dispersed in the electrolyte is self-assembled on the electrode to repair a degraded catalyst layer. The self-repairing catalyst is promising to achieve both

high OER activity and durability because the catalytic activity and durability can separately be designed. For the self-repairing catalysts, we proposed a hybrid cobalt hydroxide nanosheet (Co-ns), consisting of a brucite-type cobalt hydroxide nanosheet modified with a tripodal ligand on the surface [16]. Because of the surface functional groups, Co-ns is highly dispersible in an alkaline electrolyte and possesses high surface area. Nickel electrodes coated with Co-ns exhibited quite high durability under potential cycling conditions.

To develop simpler and cost-effective materials, we focused on iron. Iron is one of the most promising elements to be used as active and durable catalysts for OER in highly concentrated alkaline electrolytes. High durability is expected for Fe-based oxides and hydroxides because their redox reaction hardly occurs under the expected potential region (i.e., 0.5–1.8 V vs. RHE) for the anode of AWE. Because of the quite high abundance of Fe in the earth's crust, the use of Fe-based materials is advantageous to the resources and material costs. It is well known that the OER activity of Ni-based (hydr)oxides is highly improved by incorporating iron within the structure. High OER activity is expected for the combination of Fe-based (hydr)oxides and a nickel electrode. Furthermore, β-FeOOH and its composite with $Ni(OH)_2$ have been investigated as highly active OER catalysts [17-20]. Iron oxyhydroxides are also expected as OER catalysts, and β-FeOOH was predicted as the best OER catalysts among them [21].

On the other hand, we have to renew the method for the evaluation of the durability of electrodes under the repeated potential changes, simulating renewable energy. Many researchers have briefly applied cyclic voltammetry (CV) for many cycles, whereas the range of potential and the cycle numbers have not been unified yet [16]. Importantly, the potential range of CV is affected by the ohmic loss due to uncompensated resistance because the rated current density of AWE and AEMWE is usually high (typically 0.2–2 A cm^{-2}). According to our previous study on a nickel electrode, the degradation was observed from the 4000th cycle of CVs with the potential range of 0.5–1.8 V vs. RHE [16]. Recently, we have proposed a new shutdown-based accelerated durability test (SD-ADT) protocol, simulating the operation of AWE powered by renewable energies, in which current-controlled electrolysis and potential-controlled shutdown are repeated for many cycles [22]. This new protocol allows high reproducibility and application of sufficiently high stress to evaluate the durability. For example, a $NiCoO_x$ catalyst degraded in 800 cycles of the SD-ADT.

Here, we demonstrate the one-pot synthesis of ultrasmall β-FeOOH nanorod (β-FeOOH-nr), using tris(hydroxymethyl)aminomethane (denoted as Tris-NH_2) as an organic buffer and its use as an OER catalyst (Fig. 1). We found that the soft-chemically

synthesized nanostructured catalyst is useful for its unique self-repairing property. The ultrasmall nanorods were highly dispersible in an electrolyte, such as 1 M KOH aq. Dispersed β-FeOOH-nr is deposited electrochemically on an electrode to form a layer with both catalytic and protective abilities (Figs. 2a and b). Only a small amount of β-FeOOH-nr was sufficient to exhibit durability under the SD-ADT conditions and high OER activity in the presence of β-FeOOH-nr in the electrolyte. The catalyst layer is degraded under SD-ADT to expose the nickel surface (Fig. 2c). β-FeOOH-nr was continuously deposited on the electrode to protect the nickel substrate from corrosion during the SD-ADT (Figs. 2d and e). Therefore, β-FeOOH-nr is promising as highly active, durable, and cost-effective self-repairing OER catalyst for AWE powered by renewable energy.

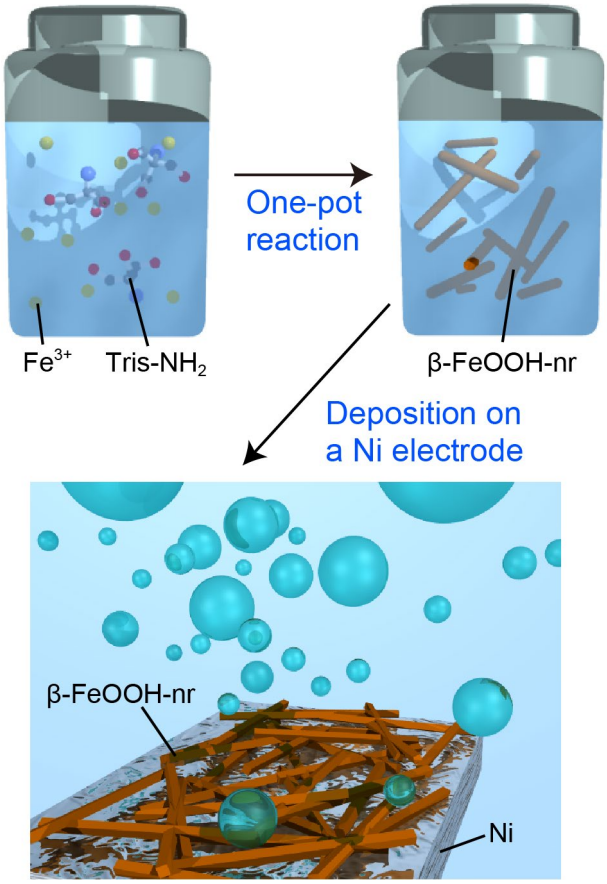

Fig. 1 Schematic illustration of the synthesis of ultrasmall β-FeOOH-nr and its use as an OER catalyst.

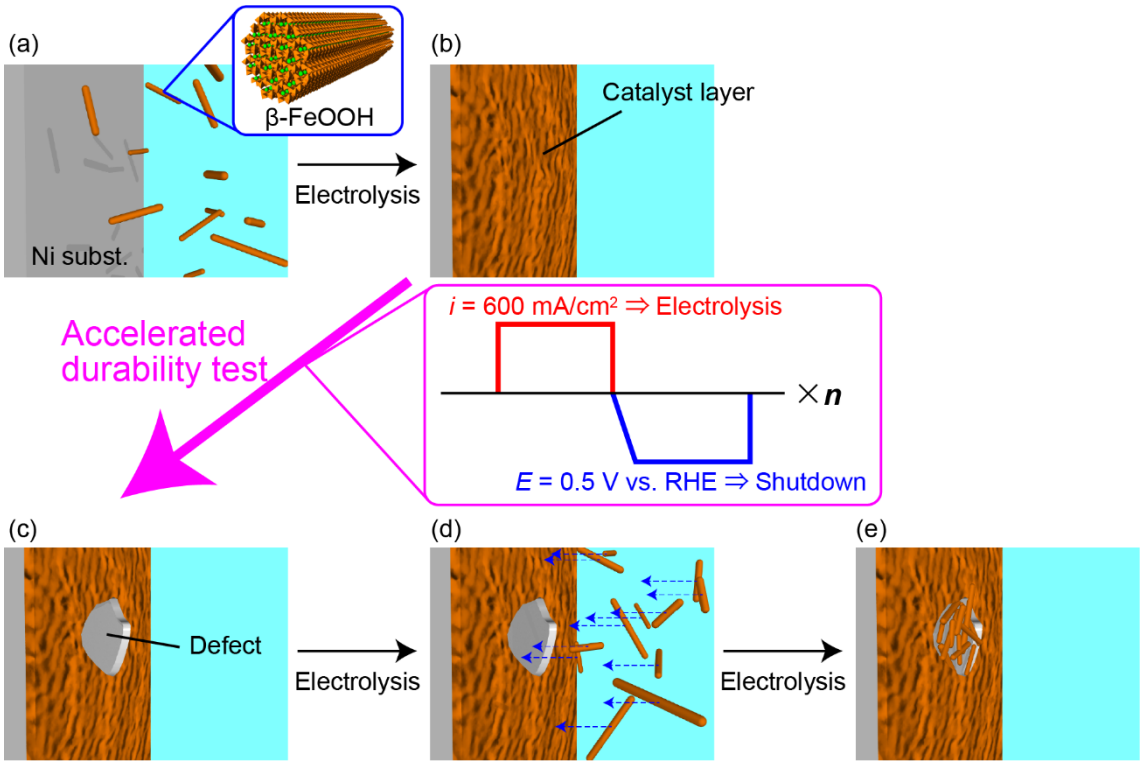

Fig. 2 Schematic illustration of proposed model of the self-repairing process. **a** nickel substrate and dispersed β-FeOOH-nr, **b** catalyst layer deposited on the nickel substrate, **c** degraded catalyst layer after the SD-ADT, **d** accumulation of β-FeOOH-nr dispersed in the electrolyte on the catalyst layer, and **e** repaired catalyst layer.

2 Experimental

2.1 Materials

Iron chloride hexahydrate ($FeCl_3 \cdot 6H_2O$) and tris(hydroxymethyl)aminomethane (denoted as Tris-NH_2 like in our previous study [23]) were purchased from FUJIFILM Wako Pure Chemical Co. and used without purification. Nickel wire was purchased from the Nilaco Co. The wire was etched in a boiling 6 M HCl aq. for 6 min. prior to the use. Co-ns was used as self-repairing catalyst for comparison. The synthetic method of Co-ns is reported elsewhere [16]. The mass percentages of Co, C, H, and N in the Co-ns were 38.9%, 13.5%, 4.2%, and 3.9%, respectively. The average particle size of the Co-ns was about 30 nm measured by SEM.

2.2 Synthesis of β-FeOOH-nr

An aqueous solution of 1 M Tris-NH_2 was mixed with an aqueous solution of 0.5 M $FeCl_3$, followed by stirring for 30 min. The mixture was poured in a tightly capped polypropylene bottle and placed in an oven at 90 °C for 48 h, and a suspension of β-FeOOH-nr was obtained. β-FeOOH-nr was collected by vacuum filtration, using a membrane filter (pore size: 0.2 μm). The collected gel was redispersed in deionized water, stirred for 30 min and then filtrated. This washing process was repeated two times. The resultant gel was used for electrochemical tests without drying. On the other hand, a part of the gel was separated and dried in an oven at 80 °C, ground on a mortar. The dried powder was used for the characterizations. The iron-based yield of β-FeOOH-nr was 32%.

2.3 Characterization

Elemental analysis of β-FeOOH-nr was performed by inductively coupled plasma atomic emission spectroscopy (ICP-AES) using an SII SPS3000 spectrometer. The samples were dissolved in nitric acid for measurements. A catalyst deposited on a nickel electrode was dissolved in a 1 M HCl aq. and then diluted to 0.1 M HCl aq. for the measurement. The CHN elemental analysis was performed by a yanaco CHN corder MT-5 instrument at A RABBIT SCIENCE. X-ray absorption near edge structure (XANES) analyses were performed at BL16B2 synchrotron radiation facility in the SPring-8 (Japan). XANES spectra were recorded at the Fe K-edge in conversion electron yield method. X-ray diffraction (XRD) patterns were collected by a Rigaku Ultima IV diffractometer, using CuKα radiation at 40 kV and 40 mA. Fourier transform infrared spectroscopy (FTIR) spectra were obtained by a JASCO FT/IR6100 using a KBr disk. Transmission electron microscopy (TEM) images were recorded using a JEOL JEM-2100F microscope at the accelerating voltage 200 kV. The samples were dispersed in ethanol and dried on a holey carbon-coated Cu microgrid. Scanning electron microscopy (SEM) images and energy dispersive X-ray spectroscopy (EDX) were collected using a JEOL JCM-7000 microscope at the accelerating voltage 15 kV. Field emission SEM (FE-SEM) images were collected using a Hitachi SU8010 microscope at the accelerating voltage 15 and 30 kV.

2.4 Instruments for electrochemical tests

Electrochemical test was performed, using a three-electrode cell composed of PFA. Ni wire, Ni coil, and reversible hydrogen electrode (RHE) are used as the working, counter, and reference electrodes, respectively. The counter electrode was covered with a

cylindrical membrane made of Zirfon Perl UTP500 (AGFA) to suppress transportation of H_2 to the working electrode [22]. Aqueous solutions of 1 and 7 M KOH purged with N_2 are used as the electrolyte at 30 ± 1 °C. Approximately 250 mL of electrolyte was poured in the cell, and 0.40 mL of the dispersion of Fe-based catalysts (25 mg/mL) were added in the electrolyte under vigorous stirring (800 rpm). The cell was connected to the BioLogic VSP-3e potentiogalvanostat for the electrochemical measurements.

2.5 Electrochemical deposition of β-FeOOH-nr

To deposit β-FeOOH-nr dispersed in the electrolyte on the working electrode (Ni wire) by constant current electrolysis, the following protocol was applied. i) Constant current electrolysis (denoted as CP) at 1000 mA cm^{-2} for 30 min, ii) cyclic voltammetry (CV) between 1.0 and 2.0 V vs. RHE at 5 mV s^{-1} for a cycle, iii) CV between 1.0 and 1.6 V vs. RHE at 50 mV s^{-1} for two cycles, and iv) electrochemical impedance spectroscopy (EIS) between 10^5 and 1 Hz with the amplitude of 15 mA cm^{-2} at the bias current density of 50 mA cm^{-2}. The uncompensated resistance of all potentials was corrected, using the solution resistance obtained by the EIS (Fig. S1). The charge of the anodic peak (Q_a) from the CV obtained by the process iii) was calculated between 1.20 and 1.50 V vs. RHE. The OER current was subtracted by the Tafel equation fitted between 1.48 and 1.49 V vs. RHE. As a control experiment, the similar protocol was applied for the coating of a nickel electrode with Co-ns, though the current density of CP was 800 mA cm^{-2} according to our previous study [16]. 0.40 mL of the dispersion of Co-ns (50 mg/mL) were added in the electrolyte. The nickel substrates coated with β-FeOOH-nr and Co-ns by 240 min of CP are hereafter denoted as β-FeOOH-nr/Ni and Co-ns/Ni, respectively.

2.6 Shutdown-based accelerated durability test

The SD-ADT was performed using a bare nickel electrode without any catalysts, Co-ns/Ni in the presence of Co-ns dispersed in the electrolyte or β-FeOOH-nr/Ni in the presence of β-FeOOH-nr dispersed in the electrolyte. The SD-ADT protocol is as follows (Fig. S2). v) CP at 600 mA cm^{-2} for 1 min, vi) potential sweep from open circuit potential to 0.5 V vs. RHE at the sweep rate of 500 mV s^{-1}, vii) keeping constant potential at 0.5 V vs. RHE for 1 min. The set of processes v)–vii) is denoted as an ADT cycle. After the processes v)–vii) were repeated for 100 cycles, the processes i)–iv) in the previous section were performed to evaluate the OER activity. The constant current electrolysis of the process i) was performed to repair the catalyst layer by accumulating the catalyst from the electrolyte. When the bare nickel electrode was used for SD-ADT, the process i) was

avoided. These cycles were repeated for 20 cycles up to the total ADT cycle of 2000 or 4000.

3 Results and discussion

3.1 Characterization of β-FeOOH nanorods

The mass percentages of Fe, C, H, N, Cl in the β-FeOOH-nr were 55.1%, 0.0%, 1.6%, 0.0%, and 7.7%, respectively. The diffractions in the XRD pattern of the β-FeOOH-nr were assigned to those of β-FeOOH (JCPDS 013-0157) (Fig. 3a). The crystallite size was estimated to be 4.8 nm by the Scherrer's equation. In the FTIR spectrum of β-FeOOH-nr, bands at 418, 679, and 846 cm^{-1} were observed (Fig. 3b). These bands are consistent with those of β-FeOOH [24]. The Fe K-edge XANES spectrum of β-FeOOH-nr exhibited the similar rising edge to that of Fe_2O_3, whereas FeO exhibited the rising edge at lower energy (Figs. 3c–e). The fitting of the spectrum of β-FeOOH-nr with those of FeO and Fe_2O_3 showed that the average oxidation number of Fe in β-FeOOH-nr was 3.0. According to the above results, the sample has the 2×2 tunnel structure of β-FeOOH in which Cl^- and water molecules are present inside the tunnels (Fig. 3a, inset). A part of O^{2-} within the FeOOH framework should be protonated to compensate the charge of Cl^-. Thus, the formula of β-FeOOH-nr is estimated to be $FeOOH_{1.22}$-$Cl_{0.22}$·$0.19H_2O$. It is said that the ideal Cl/Fe ratio of β-FeOOH is 1/8 (= 0.125) on the basis of the crystal structure [25]. The much higher Cl/Fe ratio of β-FeOOH/nr (0.22) than the ideal value, implying that much Cl^- is present not only in tunnel but also on the outer surface.

Different from the case of brucite-type metal hydroxides [23], no modification occurred on β-FeOOH, probably because the non-flat surface structure of β-FeOOH is not suited for the formation of a tridentate alkoxy linkage. A tripodal ligand forms tridentate alkoxy linkage with the surface hydroxy groups on the brucite layer due to size matching effect, though such a structural matching is not expected for the β-FeOOH and the tripodal ligands. Although β-FeOOH was not modified with the tripodal ligand, the addition of Tris-NH_2 influenced significantly on the morphology of the products as shown below.

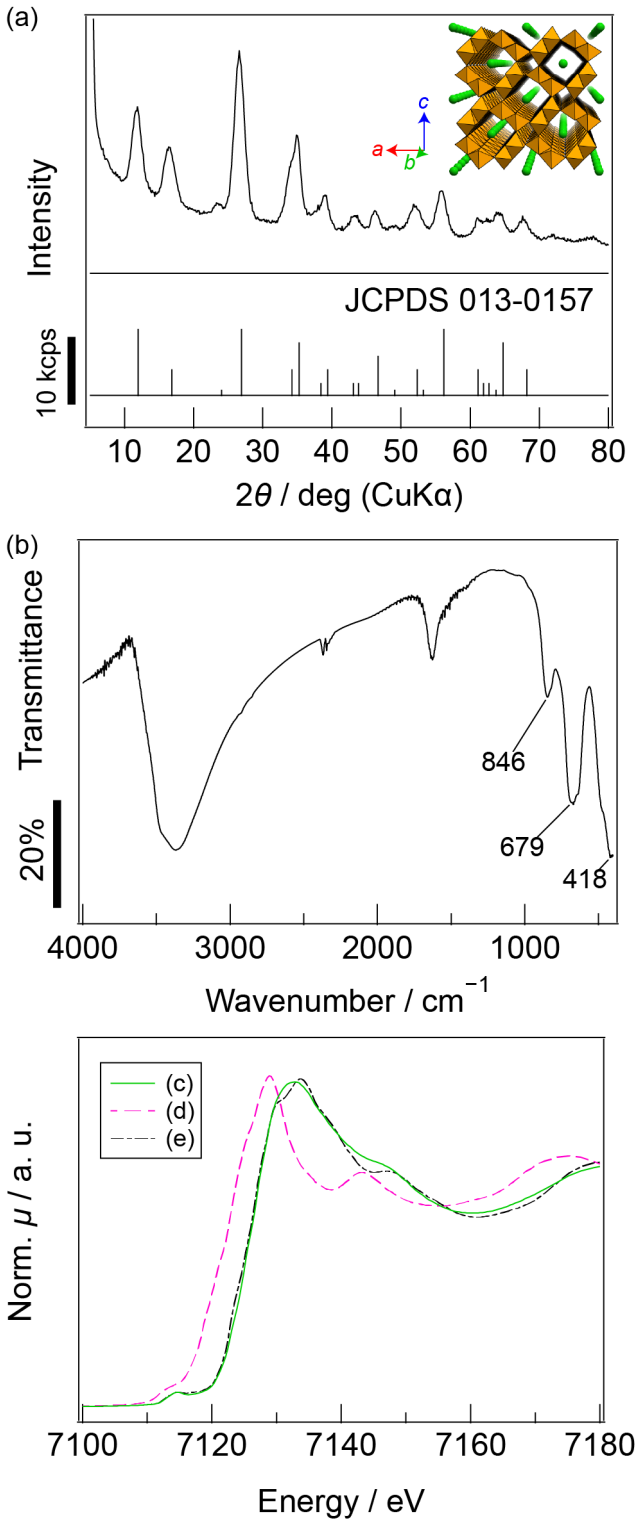

Fig. 3 **a** XRD pattern and **b** FTIR spectrum of β-FeOOH-nr. XANES spectra of **c** β-FeOOH-nr, **d** FeO, and **e** Fe_2O_3. Inset in **a** is the crystal structure of β-FeOOH. Brown octahedra represent FeO_6 units, and green spheres represent Cl^-.

The rodlike shape of the β-FeOOH-nr was observed by TEM (Fig. 4a). The width was in the range of 3–6 nm and the length was widely distributed from 4 nm to 200 nm (Figs. 4b and c). Such a rodlike shape is characteristic of β-FeOOH, though the length and width of the β-FeOOH-nr are near the smallest values among reported β-FeOOH [26]. In our previous reports [27, 28], the surface modification of layered double hydroxides with Tris-NH_2 suppressed the crystal growth, whereas it is not appropriate to apply the mechanism to the synthesis of ultrasmall β-FeOOH-nr. Because the concentration of $FeCl_3$ in the reaction solution was relatively high (0.25 M), the nucleation of β-FeOOH should occur frequently in the solution, resulting in the formation of many crystals with a small size. In addition, the pH of the solution was stable around at 10 because of the buffering action of Tris-NH_2.

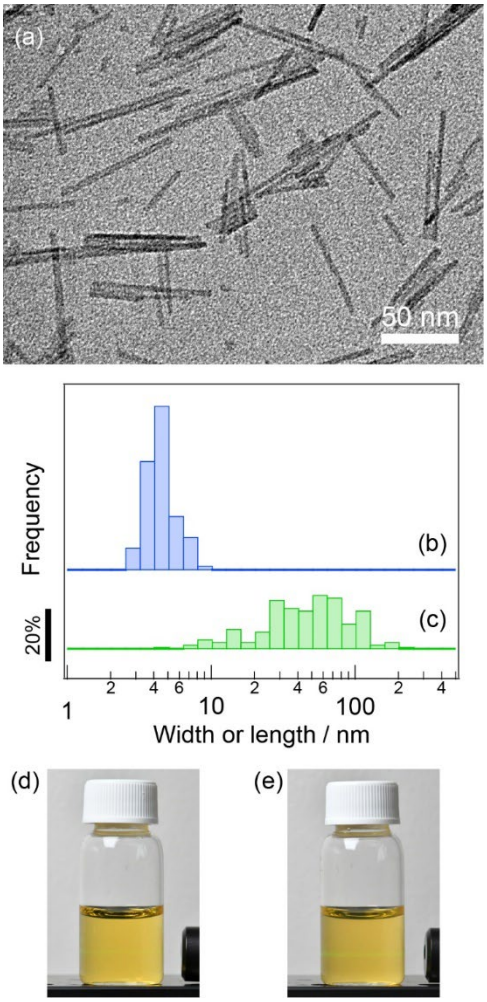

Fig. 4 **a** TEM image of β-FeOOH-nr. Size distribution of β-FeOOH-nr in **b** width and **c** length. Photographs of 40 ppm β-FeOOH-nr dispersed in **d** deionized water and **e** 1 M KOH aq. The green laser from the right exhibits Tyndall effect due to colloidal β-FeOOH-

nr

Yellow and semi-transparent dispersion of β-FeOOH-nr was obtained at the concentration of 40 ppm in both deionized water and 1 M KOH aq. (Figs. 4d and e). The Tyndall effect for the green laser indicates that colloidal β-FeOOH-nr is present in the solvent; thus, β-FeOOH-nr did not dissolve even in the highly concentrated alkaline electrolyte. The high transparency of the dispersion means that the β-FeOOH-nr are finely dispersed in water. Such a high dispersibility has also been observed for Co-ns which was used as self-repairing catalyst for OER [16, 23]. Therefore, β-FeOOH-nr is promising as a catalyst dispersible in alkaline electrolytes.

3.2 Electrochemical deposition of β-FeOOH-nr

β-FeOOH-nr was deposited on a nickel substrate by the electrolysis while OER proceeds simultaneously, which is similar to the deposition of Co-ns in our previous report [16]. The FE-SEM image of β-FeOOH-nr/Ni showed that the surface of the electrode was covered with a network of fibrous materials that consist of bundled β-FeOOH-nr nanorods (Fig. 5a). Shiny metallic surface was observed on the surface of β-FeOOH-nr/Ni (Fig. 5c) like that of a bare nickel electrode (Fig. 5f), whereas Co-ns/Ni exhibited black surface on which a thick layer of Co-ns was formed (Fig. 5h). These results mean that the deposited amount of β-FeOOH-nr was much smaller than that of Co-ns. The deposited amount of β-FeOOH-nr was only 2.00 $\mu g_{Fe} \cdot cm^{-2}$, whereas that of Co-ns was 0.128 $mg_{Co} \cdot cm^{-2}$. The fact that β-FeOOH-nr is electrochemically deposited on the nickel electrode means that β-FeOOH-nr can be used as a self-repairing catalyst to be accumulated catalyst from an electrolyte during electrolysis.

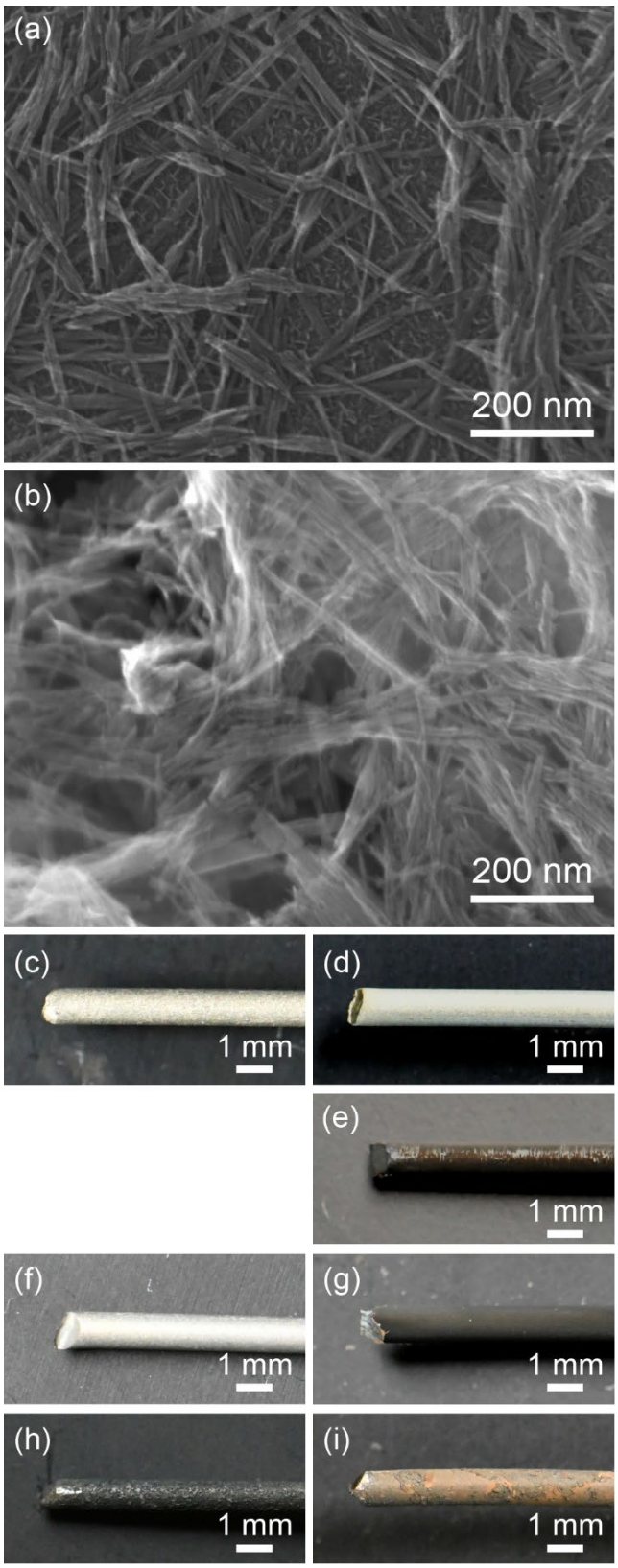

Fig. 5 FE-SEM image of β-FeOOH-nr/Ni **a** after 240 min of electrolysis for catalyst deposition and **b** after 4000 cycles of SD-ADT. Photographs of β-FeOOH-nr/Ni **c** after

240 min of electrolysis for catalyst deposition and after 4000 cycles of SD-ADT in the **d** presence and **e** absence of β-FeOOH dispersed in the electrolyte, the bare nickel electrode **f** after etching and **g** after 2000 cycles of SD-ADT, and Co-ns/Ni **h** after 240 min of electrolysis for catalyst deposition and **i** after 4000 cycles of SD-ADT.

The electric double layer capacitances (C_{dl}) of β-FeOOH-nr/Ni, Co-ns/Ni, and a bare nickel electrode were 5.1, 774, and 0.18 mF cm^{-2}, respectively. The C_{dl} value is usually proportional to the electrochemically active surface area, while pseudo capacitance due to redox of the surface hydroxide often contributes to increase in the apparent C_{dl}. Thus, the large C_{dl} value of Co-ns/Ni is due to the large amount of deposited Co-ns. The C_{dl} value of β-FeOOH-nr/Ni is much smaller than that of Co-ns/Ni and slightly higher than the bare nickel electrode. Because β-FeOOH-nr formed a thin layer on the nickel electrode, it is consistent that the electrochemically active surface area of β-FeOOH-nr/Ni is slightly higher than that of the bare nickel electrode.

The CV curve of β-FeOOH-nr/Ni exhibited only small peaks between 1.20 and 1.50 V vs. RHE (Fig. 6a), and the charge of the anodic peak (Q_a) was approximately 3 mC cm^{-2} integrated at 1.20–1.50 V vs. RHE after 240 min of electrolysis. Because the redox potential of $Fe(OH)_3 + e \rightarrow Fe(OH)_2 + OH^-$ is very low (0.266 V vs. RHE in 1 M KOH, calculated from the data reported in ref. [29]), the peak is assignable to the Ni^{2+}/Ni^{3+} redox reaction of surface hydroxide on the nickel electrode. The Q_a value of 3 mC cm^{-2} is similar to those for an oxidized bare nickel electrode. On the other hand, the CV curve of Co-ns/Ni showed large currents due to $Co^{2+/3+}$ and $Co^{3+/4+}$ redox reactions (Fig. 6a). The Q_a value was approximately 400 mC cm^{-2} integrated at 0.8–1.55 V vs. RHE after 240 min of electrolysis. The quite high Q_a value is due to the large amount of Co-ns deposited on the nickel electrode. Because the degradation of metal hydroxide catalysts is related with the repeated redox reaction to promote phase transition (e.g., β-NiOOH to γ-NiOOH [30]), β-FeOOH-nr is expected to be very stable under potential change due to reverse current.

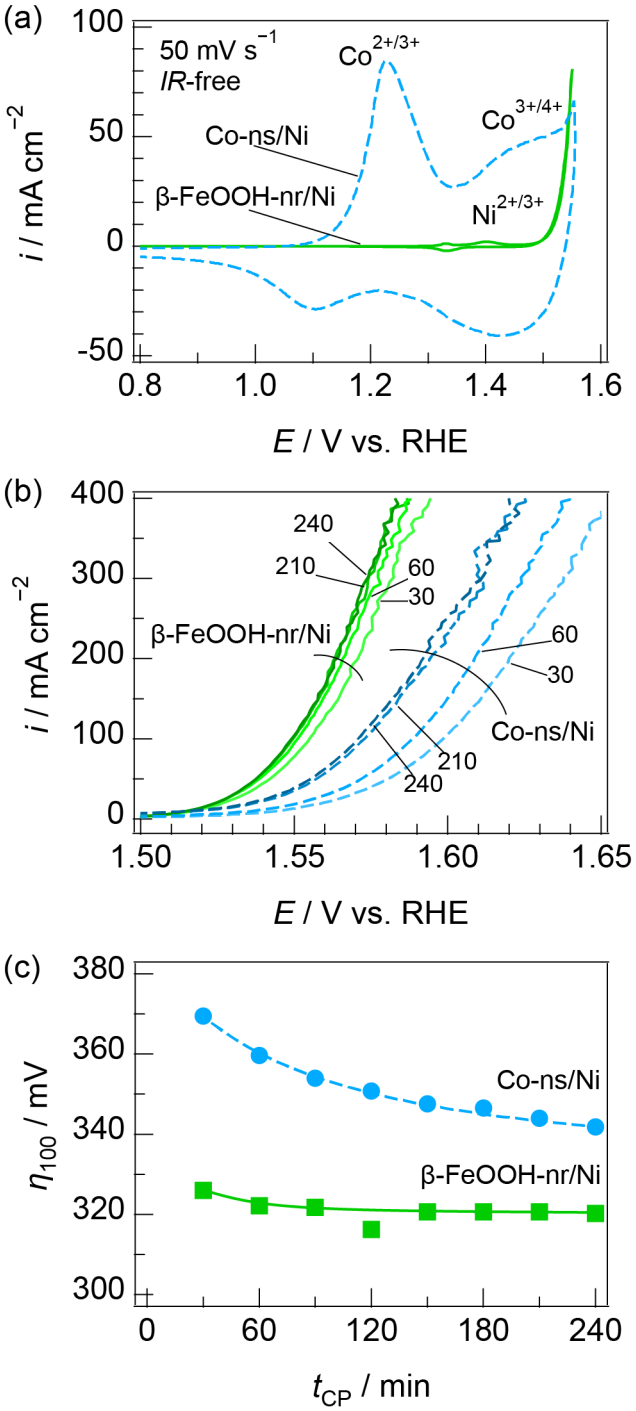

Fig. 6 **a** Cyclic voltammograms of β-FeOOH-nr/Ni and Co-ns/Ni after 240 min of electrolysis. **c** OER polarization curves of β-FeOOH-nr/Ni and Co-ns/Ni. The numbers in the graph represent the duration of CP in the unit of minute. **c** The OER overpotentials (η_{100}) of β-FeOOH-nr/Ni and Co-ns/Ni as a function of the duration of CP (t_{CP})

As we discussed previously [16], we hypothesized that Co-ns was deposited on

the surface of a nickel electrode by the anodic decomposition of organic groups. The decomposed Co-ns may lose their dispersibility and forms aggregates. Contrary, only weaker driving force was obtained for β-FeOOH-nr, containing no organic functional groups. On the surface of the nickel electrode, NiOOH is formed by the oxidation, the hydrogen bonding between β-FeOOH-nr and NiOOH possibly immobilizes β-FeOOH-nr on the surface. Further covalent bonds may also be formed among those hydroxides. Because of the weaker interparticle interactions of β-FeOOH-nr than those of Co-ns, β-FeOOH-nr possibly formed only a thin layer on the surface of a nickel substrate.

The OER polarization curves during the repeated electrolysis are shown in the Fig. 6b. The OER activity of the electrodes were improved along with the electrolysis for the deposition of catalysts. The OER overpotential at 100 mA cm^{-2} (η_{100}) was plotted as a function of the duration of electrolysis (t_{CP}) (Figs. 4e and f). When β-FeOOH-nr was used as a catalyst, low OER overpotential of 326 mV was observed at t_{CP} = 30 min and it was slightly decreased to 320 mV at t_{CP} = 240 min during the repeated electrolysis (Fig. 6c). Contrary, when Co-ns is used as a catalyst, η_{100} was gradually decreased from 370 mV at t_{CP} = 30 min to 342 mV at t_{CP} = 240 min during the repeated electrolysis. The better OER activity of β-FeOOH-nr/Ni was achieved in much shorter electrolysis time than Co-ns/Ni because β-FeOOH-nr/Ni can exhibit high OER activity from very thin catalyst layer. The final OER overpotential of β-FeOOH-nr/Ni was 22 mV lower than that of Co-ns/Ni.

3.3 Shutdown-based durability test

(1) Durability of the self-repairing catalysts

The SD-ADT was applied for β-FeOOH-nr/Ni, Co-ns/Ni, a bare nickel electrode, and a commercial $NiCoO_x$. The β-FeOOH-nr/Ni and Co-ns/Ni were tested in the presence of the dispersed catalysts (denoted as β-FeOOH-nr/Ni w/ dispersion and Co-ns/Ni w/ dispersion, respectively). The β-FeOOH-nr/Ni was also tested in the absence of the dispersed catalyst (denoted as β-FeOOH-nr/Ni w/o catalyst). The η_{100} value was plotted as a function of the ADT cycle in Fig. 7a. The bare nickel electrode showed the increase in the η_{100} value at the early stage of SD-ADT. The η_{100} value reached 530 mV at the 50th cycle and 620 mV at the 200the cycle (Fig. 7a). It is evident that the SD-ADT drastically promotes degradation of nickel due to repeated potential changes, simulating renewable energy. For example, it took approximately 10000 cycles to reach the η_{100} value of 500 mV by rapid potential cycling (potential range: 0.5–1.8 V vs. RHE, sweep rate 500 mV s^{-1}) [16].

We applied the SD-ADT method for Co-ns/Ni while CP at 800 mA cm^{-2} for 60

min was applied at every 100 ADT cycles to repair the catalyst, and found that Co-ns/Ni exhibited stable OER activity up to 2000th cycle (Fig. 7a). Because it seemed degrading after the 2000th cycle, we added another Co-ns (equivalent to 30 ppm in the electrolyte) at the 2800th cycle. The OER overpotential became stable after the addition. The degradation occurs if Co-ns is lost in the electrolyte, whereas the repairing ability is regenerated only by adding the catalyst in the electrolyte.

β-FeOOH-nr/Ni showed very low η_{100} value during 4000 cycles (Fig. 7a). No additional β-FeOOH-nr was necessary to suppress the increase in overpotential probably because the required amount of β-FeOOH-nr to cover the nickel electrode is much smaller than that of Co-ns. The OER overpotential was the smallest (247 mV at 10 mA cm^{-2} and 285 mV at 100 mA cm^{-2}) at the 2000th cycle, which is comparable to the most active NiFe LDHs [31]. Our previous report also showed that a $NiCoO_x$ anode degraded within 1000 ADT cycles (Fig. 7a). β-FeOOH-nr/Ni exhibited quite high durability under potential changes.

To assess the effect of β-FeOOH-nr dispersed in the electrolyte during SD-ADT, the SD-ADT of β-FeOOH-nr/Ni in a fresh KOH electrolyte without dispersed β-FeOOH-nr was performed (Fig. 7a). The η_{100} value increased during the 1000 ADT cycles from 380 to 528 mV, which is similar to the behavior of the $NiCoO_x$ anode. These results show that the β-FeOOH-nr dispersed in the electrolyte is deposited to repair the β-FeOOH-nr layer during the SD-ADT. Consequently, β-FeOOH-nr is a self-repairing catalyst which exhibits higher OER activity and lower requirement for amount than Co-ns.

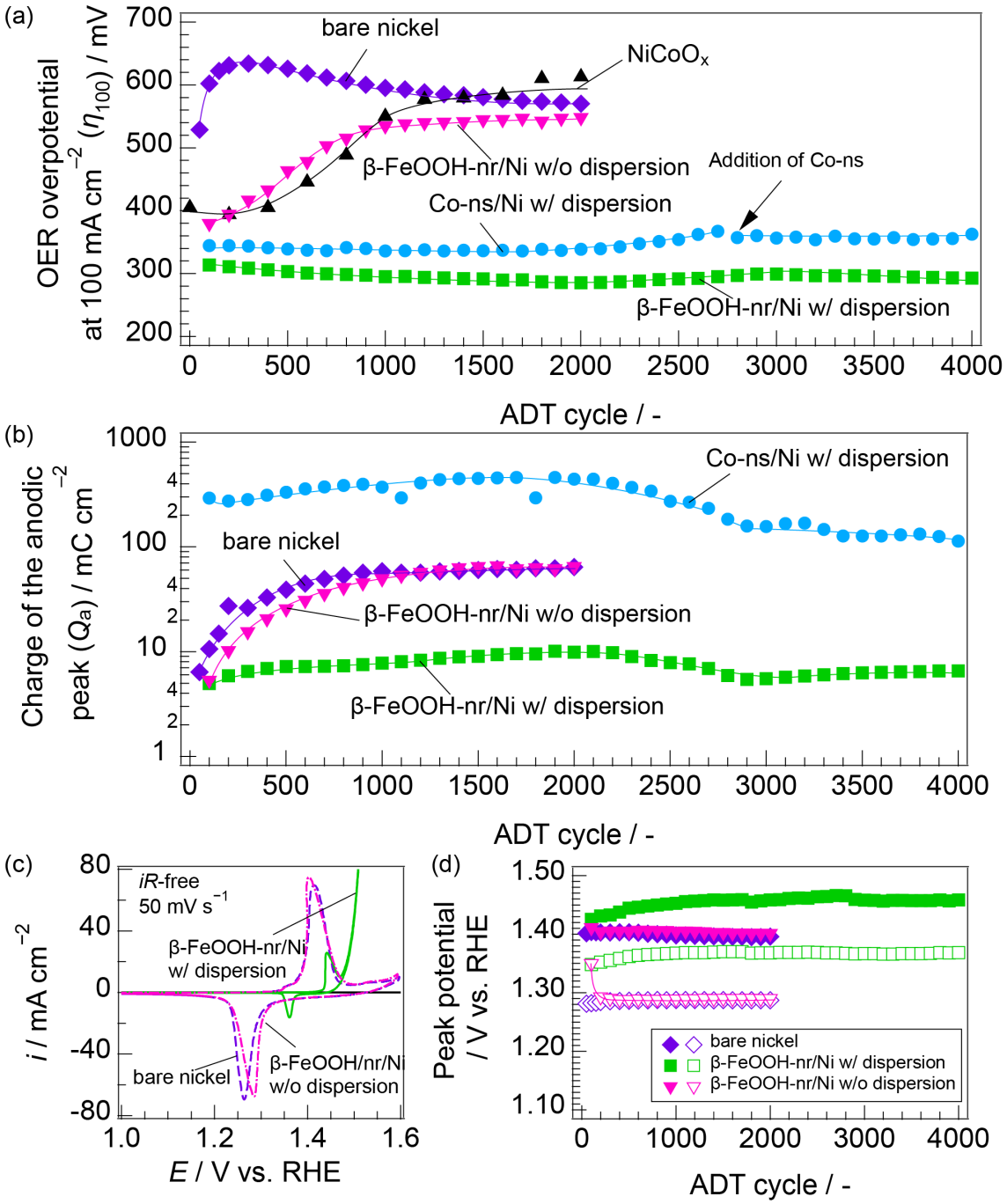

Fig. 7 Results of SG-ADT. **a** OER overpotential at 100 mA cm^{-2} (η_{100}), **b** charge of the anodic peak (Q_a), **c** cyclic voltammogram at the 2000th cycle, and **d** the peak potential in the cyclic voltammogram. The samples are bare nickel electrode, Co-ns/Ni w/ dispersion, β-FeOOH-nr/Ni w/ dispersion, NiCoO$_x$ anode from ref [22], and β-FeOOH-nr/Ni w/o dispersion.

The Q_a value of the electrodes were plotted as a function of the ADT cycle (Fig.

7b). The bare nickel electrode exhibited increase in the Q_a value from 6 mC cm^{-2} at the 50th cycle to approximately 50 mC cm^{-2} at the 2000th cycle. This increase corresponds to the evolution of surface oxidized layer consisting of $Ni(OH)_2$, NiOOH, and hydrous nickel oxides with higher oxidation number together with the decrease in the OER activity [30]. The Co-ns/Ni exhibited the highest Q_a value throughout the SD-ADT because of the deposition of large amount of catalyst. The Q_a value decreased after the 2000th cycle together with the slight decrease in the OER activity. However, after the addition of another Co-ns in the electrolyte at the 2800th cycle, the Q_a value remained low. It implied that the replacement of the Co-ns with a fresh one on the surface of the catalyst layer possibly influenced the OER activity.

Surprisingly, β-FeOOH-nr/Ni exhibited quite small Q_a (5–10 mC cm^{-2}) throughout the 4000 cycles of SD-ADT in the presence of dispersed β-FeOOH-nr (Fig. 7b). It means that the oxidation of the nickel electrode was effectively suppressed by the coating with β-FeOOH-nr. When the SD-ADT of β-FeOOH-nr/Ni was performed in the fresh KOH electrolyte without dispersed β-FeOOH-nr, the Q_a value increased like the bare nickel electrode. Therefore, the repair of the β-FeOOH-nr layer is important to suppress the corrosion of the nickel electrode. Tentatively, we hypothesized that the porous β-FeOOH-nr layer prohibited the formation of nickel hydroxides on the surface because there is less space on the nickel substrate.

(2) Active species of the β-FeOOH-nr/Ni electrode

The CV curves of the bare nickel electrode, β-FeOOH-nr/Ni in the presence and absence of β-FeOOH-nr dispersed in the electrolyte at the 2000th cycle are shown in the Fig. 7c. The peak positions of the bare nickel electrode and β-FeOOH-nr/Ni in the presence of β-FeOOH-nr dispersed in the electrolyte are obviously different from each other throughout the SD-ADT (Fig. 7d). The β-FeOOH-nr/Ni exhibited the redox peaks at higher potential (anodic: 1.44 V vs. RHE, cathodic: 1.36 V vs. RHE) than those of the bare nickel electrode (anodic: 1.41 V vs. RHE, cathodic: 1.26 V vs. RHE). Such a high-potential peak has been observed for $Ni(OH)_2$/β-FeOOH composites [32]. The $Ni(OH)_2$/β-FeOOH composites have been reported as highly active OER catalysts [18, 20, 32, 33]. Therefore, the high OER activity of β-FeOOH-nr/Ni is probably due to the in-situ formation of highly active $Ni(OH)_2$/β-FeOOH composites due to the deposition of β-FeOOH-nr and the oxidation of a small amount of nickel electrode on the surface. The peak potential was almost constant for the bare nickel electrode, whereas those of β-FeOOH-nr/Ni was increased during the 2000 ADT cycles. These results suggest that the gradual structural change of the active catalytic materials occur during the SD-ADT. The

peak potentials of β-FeOOH-nr/Ni in the absence of β-FeOOH-nr dispersed in the electrolyte showed the similar value to those of β-FeOOH-nr/Ni in the presence of β-FeOOH-nr dispersed in the electrolyte only at the 100th cycle. After that, it showed the similar peak potentials to those of the bare nickel electrode. These results support that the β-FeOOH-nr layer peeled off during the SD-ADT.

Although the high durability of β-FeOOH-nr/Ni originates from the intrinsic stability and self-repairing behavior of β-FeOOH-nr, there are changes in the cyclic voltammogram and OER activity. It is necessary to analyze β-FeOOH-nr and nickel species separately. The surface appearance of β-FeOOH-nr/Ni after 4000 ADT cycles in the presence of β-FeOOH-nr dispersed in the electrolyte was shiny silver (Fig. 5d), being almost unchanged from the as-prepared form. On the other hand, β-FeOOH-nr/Ni after 4000 ADT cycles in the absence of β-FeOOH-nr dispersed in the electrolyte was dappled black and brown (Fig. 5e), which is similar to that of the bare nickel electrode after 2000 ADT cycles (Fig. 5g). The surface appearance of Co-ns/Ni was brown and dappled (Fig. 5i), indicating the retainment of the catalyst layer. The FE-SEM image of β-FeOOH-nr/Ni after 4000 ADT cycles showed fibrous β-FeOOH-nr (Fig. 5b). The fibrous morphology indicates the retainment of the crystal structure. The surface of the nickel electrode was not observed because of the increased thickness of the β-FeOOH-nr coating (see also Fig. S3 for low magnification images.). The Fe/Ni molar ratio of β-FeOOH-nr/Ni measured by SEM–EDX increased from 0.014 to 0.053 during the 4000 ADT cycles, implying that the deposited amount of β-FeOOH-nr is around 7.6 $\mu g_{Fe} \cdot cm^{-2}$. The value is approximately four times higher than that before SD-ADT, and it is consistent with the change in the FE-SEM images. The increase in the amount of deposited β-FeOOH-nr corresponds to an excessive repair of β-FeOOH-nr layer during SD-ADT. It should be noted that the value is still quite low, compared with the thicker catalyst layer of Co-ns. Therefore, the structure and layer thickness of β-FeOOH-nr is basically unchanged during the SD-ADT.

The current density at 1.52 V vs. RHE ($i_{1.52}$) was plotted as a function of the charge of anodic redox peak (Q_a) due to nickel species (Figs. 8a and b). The $i_{1.52}/Q_a$ ratio is virtually proportional to the OER activity of electrochemically active nickel species (i.e., turnover frequency of OER). The $i_{1.52}/Q_a$ ratio is constant if the change in the catalytic activity is not due to the change in the chemical nature of the active site but due to the change in the number of active sites. There are several linear regions with different slopes. The change in the slope of linear regions should be related to the qualitative change in the catalytically active sites. Thus, we take the slope of each line as an indicator of the OER activity of active site.

The plots are divided into five regions, (i) catalyst formation step from 30 to 240

min of the electrolysis, (ii) initial steps of SD-ADT from the 100th to the 300th cycles, (iii) middle activating steps of SD-ADT from the 1000th to the 2000th cycles, (iv) middle declining steps of SD-ADT from the 2000th to the 3000th cycles, and (v) final steps of SD-ADT with relatively small changes in activity. The slopes of the regions (i), (ii), (iii), (iv), and (v) are 12, 7, 26, 15, and 26 A C_{cat}^{-1}, respectively, indicating that the OER activity of active sites changed during the SD-ADT. The redox peaks in the CV curves provide the information on the state of the active sites. Two anodic peaks appeared at 1.33 and 1.40 V vs. RHE in the region (i) (Fig. 8c). The potential of the latter one is similar to that of surface hydroxides of the bare nickel electrode (1.41 V vs. RHE). The peaks shifted to 1.41 (weak) and 1.43 (strong) V vs. RHE in the region (ii) (Fig. 8d), implying the formation of $Ni(OH)_2$/β-FeOOH-nr composites. The peak was further shifted to 1.45 V vs. RHE before the region (iii) (Fig. 8e) and the potential of the peak was almost unchanged in the regions (iii)–(v) (Figs. 8f and g). Therefore, the active nickel species are formed until the 1000th cycle and the change in the activity is mainly due to the change in the number of active sites after the 1000th cycle.

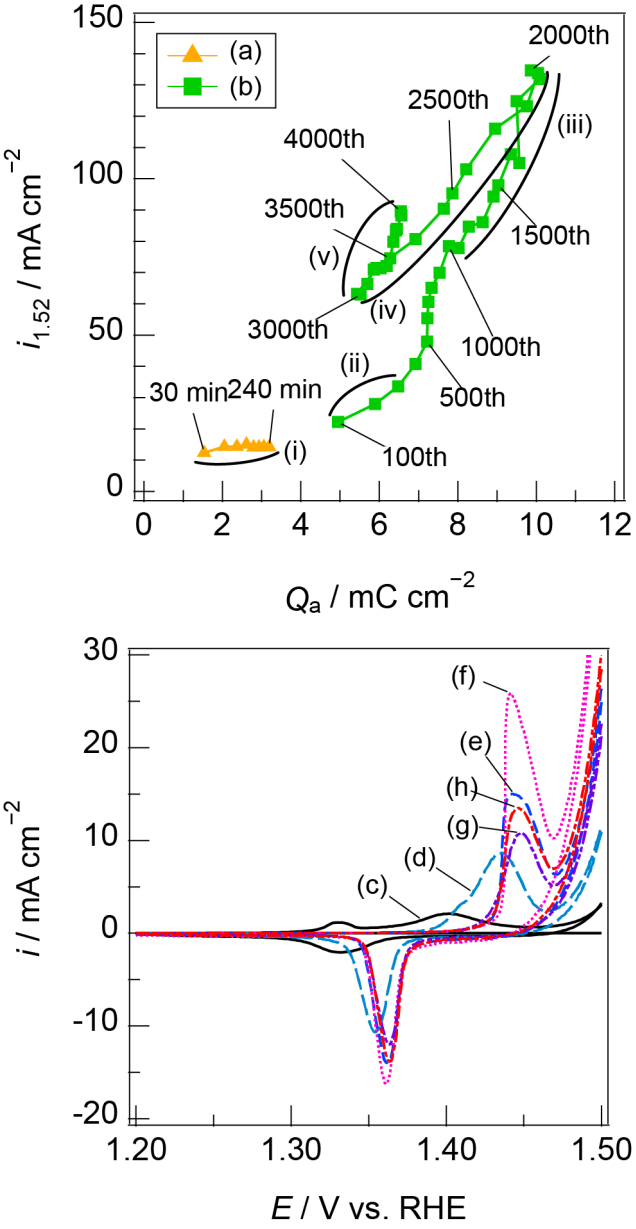

Fig. 8 Current density at 1.52 V vs. RHE of β-FeOOH-nr/Ni as a function of the charge of anodic redox peak during **a** the electrolysis for catalyst deposition and **b** the SD-ADT. CV curves of β-FeOOH-nr/Ni after **c** 240 min of electrolysis for catalyst deposition, **d** 300 ADT cycles, **e** 1000 ADT cycles, **f** 2000 ADT cycles, **g** 3000 ADT cycles, and **h** 4000 ADT cycles.

The excessive corrosion of the nickel electrode is suppressed by the deposition of β-FeOOH-nr and the protective ability is maintained due to the high stability of β-FeOOH-nr. The activity of β-FeOOH-nr/Ni is mainly governed by the active nickel species formed by the partial anodic oxidation of the nickel electrode. The active nickel

species, such as $Ni(OH)_2$, is simultaneously combined with β-FeOOH-nr to enhance the OER activity. Therefore, the β-FeOOH-nr and nickel species act as protecting and active materials, respectively.

4. Conclusion

In conclusion, purely inorganic β-FeOOH-nr was found to be useful as a self-repairing anode catalyst for alkaline water electrolysis powered by fluctuating renewable energy. β-FeOOH-nr formed thin layer to protect the nickel substrate from corrosion. The SD-ADT of the nickel electrode coated with β-FeOOH-nr in the presence of β-FeOOH-nr dispersed in the electrolyte showed quite high durability due to self-repair of the β-FeOOH-nr layer. The OER activity is probably governed by the active nickel species, combined with β-FeOOH-nr. The composite electrode exhibits not only self-repairing ability under frequent shutdown but also high OER activity. β-FeOOH-nr/Ni is useful for alkaline water electrolysis because of its low cost, abundant resource in nature, and high activity and durability.

Acknowledgement

The synchrotron radiation experiments were performed at the BL16B2 of SPring-8 with approval of the Japan Synchrotron Radiation Research Institute (JASRI) (Proposal No. 2021A5310). Part of this study uses outcomes of the development of fundamental technology for the advancement of water electrolysis hydrogen production in the advancement of hydrogen technologies and utilization projects (grant number JPNP14021) commissioned by the New Energy and Industrial Technology Development Organization (NEDO) in Japan.

Reference

[1] Götz M, Lefebvre J, Mörs F, Koch AM, Graf F, Bajohr S, Reimert R, Kolb T (2016) Renewable power-to-gas: A technological and economic review. Ren Energy 85:1371–1390

[2] Zeng K, Zhang D (2010) Recent progress in alkaline water electrolysis for hydrogen production and applications. Prog Energy Combust. Sci. 36:307–326

[3] Carmo M, Fritz DL, Mergel J, Stolten D (2013) A comprehensive review on PEM water electrolysis. Int J Hydrogen Energy 38:4901–4934

[4] Jamesh MI, Sun X (2018) Recent progress on earth abundant electrocatalysts for

oxygen evolution reaction (OER) in alkaline medium to achieve efficient water splitting – A review. J Power Source 400:31–68.
[5] Holmin S, Näslund LÅ, Ingason ÁS, Rosen J, Zimmerman E (2014) Corrosion of ruthenium dioxide based cathodes in alkaline medium caused by reverse currents. Electrochim Acta 146:30–36
[6] Uchino Y, Kobayashi T, Hasegawa S, Nagashima I, Sunada Y, Manabe A, Nishiki Y, Mitsushima S (2018) Relationship between the redox reactions on a bipolar plate and reverse current after alkaline water electrolysis. Electrocatalysis 9:67–74
[7] Uchino Y, Kobayashi T, Hasegawa S, Nagashima I, Sunada Y, Manabe A, Nishiki Y, Mitsushima S (2018) Dependence of the reverse current on the surface of electrode placed on a bipolar plate in an alkaline water electrolyzer. Electrochemistry 86:138–144
[8] Miller HA, Bouzek K, Hnat J, Loos S, Bernäcker CI, Weiβgärber T, Röntzsch L, Meier-Haack J (2020) Green hydrogen from anion exchange membrane water electrolysis: a review of recent developments in critical materials and operating conditions. Sustainable Energy Fuels 4:2114–2133
[9] Yu M, Budiyanto E, Tüysüz H (2022) Principles of water electrolysis and recent progress in cobalt, nickel, and iron-based oxides for the oxygen evolution reaction. Angew Chem Int Ed 61:e202103824
[10] Fujita S, Nagashima I, Sunada Y, Nishiki Y, Mitsushima S (2017) Electrocatalytic activity and durability of $Li_xNi_{2-x}O_2$/Ni electrode prepared by oxidation with LiOH metl for alkaline water electrolysis. Electrocatalysis 8:422–429
[11] Fujita S, Nagashima I, Nishiki Y, Canaff C, Napporn TW, Mitsushima S (2018) The effect of $Li_xNi_{2-x}O_2$/Ni with modification method on activity and durability of alkaline water electrolysis anode. Electrocatalysis 9:162–171
[12] Todoroki N, Wadayama T (2019) Heterolayered Ni-Fe hydroxide/oxide nanostrucures generated on a stainless-steel substrate for efficient alkaline water splitting. ACS Appl Mater Interface 11:44161–44169
[13] Todoroki N, Wadayama T (2021) Electrochemical stability of stainless-steel-made anode for alkaline water electrolysis: Surface catalyst nanostructures and oxygen evolution overpotentials under applying potential cycle loading. Electrochem Commun 122:106902
[14] Todoroki N, Shinomiya A, Wadayama T (2022) Nanostructures and oxygen evolution overpotentials of surface catalyst layers synthesized on various austenitic stainless steel electrodes. Electrocatalysis, in press.
[15] Barwe S, Masa J, Andronescu C, Mei B, Schuhmann W, Ventosa E (2017) Overcoming the instability of nanoparticle-based catalyst films in alkaline electrolyzers

by using self-assembling and self-healing films. Angew Chem Int Ed 56:8573–8577
[16] Kuroda Y, Nishimoto T, Mitsushima S (2019) Self-repairing hybrid nanosheet anode catalysts for alkaline water electrolysis connected with fluctuating renewable energy. Electrochim Acta 323:134812
[17] Suzuki TM, Nonaka T, Suda A, Suzuki N, Matsuoka Y, Arai T, Sato S, Morikawa T (2017) Highly crystalline β-FeOOH(Cl) nanorod catalysts doped with transition metals for efficient water oxidation. Sustainable Energy Fuels 1:636–643
[18] Suzuki TM, Nonaka T, Kitazumi K, Takahashi N, Kosaka S, Matsuoka Y, Sekizawa K, Suda A, Morikawa T (2018) Highly enhanced electrochemical water oxidation reaction over hyperfine β-FeOOH(Cl):Ni nanorod electrode by modification with amorphous $Ni(OH)_2$. Bull Chem Soc Jpn 91:778–786
[19] Sakamoto Y, Noda Y, Ohno K, Koike K, Fujii K, Suzuki TM, Morikawa T, Nakamura S (2019) First principles calculations of surface dependent electronic structures: a study on β-FeOOH and γ-FeOOH. Phys Chem Chem Phys 21:18486–18494
[20] Morikawa T, Gul S, Nishimura YF, Suzuki TM, Yano J (2020) Operando X-ray absorption spectroscopy of hyperfine β-FeOOH nanorods modified with amorphous $Ni(OH)_2$ under electrocatalytic water oxidation conditions. Chem Commun 56:5158–5161
[21] Huang Z, Han F, Li M, Zhou Z, Guan X, Guo L (2019) Which phase of iron oxyhydroxides (FeOOH) is more competent in overall water splitting as a photocatalyst, goethite, akaganeite or lepidocrocite? A DFT-based investigation. Compt Mater Sci 169:109110
[22] Abdel Haleem A, Nagasawa K, Kuroda Y, Nishiki Y, Zaenal A, Mitsushima S (2021) A new accelerated durability test protocol for water oxidation electrocatalysts of renewable energy powered alkaline water electrolyzers, Electrochemistry 89:186–191
[23] Kuroda Y, Koichi T, Muramatsu K, Yamaguchi K, Mizuno N, Shimojima A, Wada H, Kuroda K (2017) Direct synthesis of highly designable hybrid metal hydroxide nanosheets by using tripodal ligand as one-size-fits-all modifiers. Chem Eur J 23:5023–5032
[24] Sklute EC, Kashyap S, Dyar MD, Holden JF, Tague T, Wang P, Jaret SJ (2018) Spectral and morphological characteristics of synthetic nanophase iron (oxyhydr)oxides. Phys Chem Miner 45:1–26
[25] Kaneko K, Serizawa M, Ishikawa T, Inouye K (1975) Dielectric behavior of water molecules adsorbed on iron(III) oxide hydroxides. Bull Chem Soc Jpn 48:1764–1769
[26] Akharame MO, Fagbayigbo BO, Pereao O, Oputu OU, Olorunfemi DI, Fatoki OS, Opeolu BO (2021) Beta-FeOOH nanoparticles: a promising nano-based material for

water treatment and remediation. J Nanoparticle Res 23:8
[27] Kuroda Y, Miyamoto Y, Hibino M, Yamaguchi K, Mizuno N (2013) Tripodal ligand-stabilized layered double hydroxide nanoparticles with highly exchangeable CO_3^{2-}. Chem Mater 25:2291–2296
[28] Kuroda Y, Oka Y, Yasuda T, Koichi T, Muramatsu K, Wada H, Shimojima A, Kuroda K (2018) Precise size control of layered double hydroxide nanoparticles through reconstruction using tripodal ligands. Dalton Trans 47:12884–12892
[29] Milazzo G, Caroli S (1978) Tables of standard electrode potentials, Wiley-Interscience, New York
[30] Lyons MEG, Doyle RL, Godwin I, O'Brien M, Russell L (2012) Hydrous nickel oxide: Redox switching and the oxygen evolution reaction in aqueous alkaline solution. J Electrochem Soc 159:H932–H944
[31] Wang Y, Yan D, Hankari SE, Zou Y, Wang S (2018) Recent progress on layered double hydroxides and their derivatives for electrocatalytic water splitting. Adv Sci 5:1800064.
[32] Zhu K, Luo W, Zhu G, Wang J, Zhu Y, Zou Z, Wei H (2017) Interface-engineered $Ni(OH)_2$/β-like FeOOH electrocatalysts for highly efficient and stable oxygen evolution reaction, Chem Asian J 12:2720–2726
[33] Niu S, Sun Y, Sun G, Rakov D, Li Y, Ma Y, Chu J, Xu P (2019) Stepwise electrochemical construction of FeOOH/$Ni(OH)_2$ on Ni foam for enhanced electrocatalytic oxygen evolution, ACS Appl Energy Mater 2:3927–3935

Statements & Declarations

Funding

This work was supported by the JSPS KAKENHI (grant number 20H02821) from Ministry of Education, Culture, Sports, Science and Technology (MEXT) Japan.

Conflict of interests

The authors have no relevant financial or non-financial interests to disclose.

Author contributions

Y. K. and S. M. designed the experiments. Y. K. performed electrochemical experiments and wrote the draft of manuscript. S. T. performed the synthesis of samples and electrochemical experiments under the supervision of Y. K. and S. M. T. T., Y. S., I. N. and A. I. analyzed the samples at the Synchrotron facility. Y. N., A. Z., T. N., and A. K. performed electrochemical experiments. All authors contributed to the review of the final manuscript.